IOMAC'15
6th International Operational Modal Analysis Conference
2015 May12-14 Gijón - Spain

AUTOMATIC OPERATIONAL MODAL ANALYSIS FOR AEROELASTIC APPLICATIONS

Jan Schwochow[1], *and Goran Jelicic*[2]

[1] Scientist, DLR – Institute of Aeroelasticity, Bunsenstraße10, 37073 Göttingen, Germany, jan.schwochow@dlr.de.
[2] Scientist, DLR – Institute of Aeroelasticity, Bunsenstraße10, 37073 Göttingen, Germany, goran.jelicic@dlr.de.

ABSTRACT

The development of new aircraft requires the evaluation of the aeroelastic stability to avoid the phenomenon of flutter, a self-excited oscillation of the airframe. Since the rational analysis of the flutter stability comprises coupled simulations using numerical structural models and unsteady aerodynamic loads, the accomplishment is complex and the implementations must be checked for their validity by comparison of analytical and experimental results. In the so-called Ground Vibration Test (GVT) the natural modes, eigenfrequencies and damping ratios of the prototype aircraft are identified using classical Experimental Modal Analysis (EMA) methods. Depending on the complexity of the new design, conducting such a test requires a time slot of several days shortly before the first flight. Consequently, there is an ongoing need to reduce the testing time to improve the availability of the aircraft prototype.

This paper addresses the application of Operational Modal Analysis (OMA) methods during the GVT of an aircraft, which might cut down the efforts in time and labour. An automatically running fast implementation of the Stochastic Subspace Identification method (SSI) is introduced, which analyses the output acceleration response of the airframe randomly excited by modal shakers. The identification process is specified in detail for a glider aircraft, where acceleration time series must be evaluated to generate the stabilization diagram. To isolate the physical mode shapes from the mathematical poles, a pole-weighted Modal Assurance Criteria (MAC) is evaluated for several model orders to clean the stabilization diagram. Since the process needs no further operator interaction, it is suitable for monitoring airframe vibrations of the aircraft in flight, provided that the changes in flight conditions are significantly slower than the duration of the vibration periods considered. For the sucess of the methods, the OMA requirements should be fulfilled, i.e. the excitation of aircraft should be non-deterministic with broad-band spectra. Such conditions are provided by atmospheric turbulence excitation and/or pilot control inputs. The presented autonomous process is applied to a simulated Flight Vibration Test (FVT) of an research aircraft with real-time modal identification where changes of eigenfrequencies and damping ratios are tracked with changes in flight conditions.

Keywords: Operational Modal Analysis, Aeroelasticity, Ground Vibration Test, Flight Vibration Test

1. INTRODUCTION

Flutter is a dynamic instability caused by the interaction of the structural dynamics of the aircraft and unsteady aerodynamic forces. It occurs when one of the elastic modes of the aircraft tends to negative

damping above a critical flutter speed. Flutter prediction and flutter clearance are important problems in the design, development and certification of aircraft. From a practical point of view, Flight Vibration Testing (FVT) needs to be performed whenever a new aircraft is built or an existing aircraft is modified. The procedure of demonstrating that the aircraft is free from flutter in the specified range of velocities and altitudes is called flight envelope clearance. Efficient and reliable methods of flutter testing could save a lot of flight time. As a prerequisite for FVT, it is required to measure the modal parameters of the airframe comprising eigenfrequencies, damping ratios and mode shapes without aerodynamic forces in the Ground Vibration Test (GVT). The modal parameters from the GVT are used to verify the numerical structural model, which is based on the Finite Element Method (FEM).

Conventional methods for FVT consist of estimating eigenfrequencies and damping ratios of the aeroelastic modes against the flight speed. The flutter speed is mainly determined by extrapolation of the damping at subcritical speeds. Since damping characteristics often change abruptly near the flutter boundary, it is necessary to evaluate them up to speeds which are very close to the stability boundary. An overview of FVT can be found in [1], while an example on how to perform the FVT, is documented in [2]. There, the in-flight identification of the modal parameters is still limited to single degree of freedom methods and requires interaction by an operator. The application of automatic Operational Modal Analysis (OMA) methods may provide improvements to identify modal parameters of multiple modes in one step. If the identification is repeated for increasing flight velocities, it is possible to find the aeroelastic damping trends and to extrapolate to the stability boundary.

During the last decades considerable effort has been put into the construction of algorithms for estimation of the parameters in MIMO (multi-input multi-output) state-space systems, see e.g. Van Overschee and De Moor [3]. One of the first utilization of the real-time modal parameter estimation can be found in references [4] and [5], where the so-called subspace methods come into operation to identify a truss framework. The Stochastic Subspace Identification (SSI) method is explained by Brincker and Andersen in [6]. The so-called stabilization diagram is a GUI-assisted way to support the operator in separating the physical poles from the mathematical ones in the subspaces. In [7] several algorithms are presented for establishing fast multi-order state-space systems with minimized computational effort, while references [8] and [9] explain methods for the automatic selection of the poles without manual interaction, which is a requirement for the automatic online-monitoring of vibration.

In case of wind tunnel testing the structural integrity of flexible airfoils or even complete aircraft needs to be assured for the test campaign because a failure can cause severe damage on the wind tunnel facility. A fast and reliable online identification procedure of eigenfrequencies and damping ratios was developed in [10] and has been applied to predict flutter critical speeds in a wind tunnel test campaign. An elastically suspended 2D airfoil was tested in the so-called flutter test rig with 2 degrees of freedom for pitch and heave motion. Besides the very fast realization of the well-known Least-Square Complex Frequency (LSCF) estimator, the numerical implementation of the SSI method is available, which is presented in section 3, where the strategy to clean the stabilization diagrams is shortly reviewed. For further demonstration of the performance capabilities, the presented automatic OMA procedure is applied to the structural acceleration time series measured during the GVT of a glider aircraft in section 4.1 and to the recorded in-flight vibration signals of an instrumented research aircraft, where a scientific modification was under investigation during a FVT in section 4.2.

2. OBJECTIVES

A fully automatic process for the OMA application is presented to identify the modal parameters eigenfrequencies, dampings ratios and mode shapes of an aeroelastic system, which includes the fluid-structure coupling. Thus, the well known state-space description of a structural system is expanded with the vibration-induced aerodynamic forces. These introduce additional lag states to characterize the time delay between the motion of the airframe and the aerodynamic forces induced. With this assumptions the well-known SSI technique can be applied to aeroelastic systems, where the modal parameters are dependent on the flight condition comprising flight speed, Mach number and atmospheric density of the incoming flow. Therefore, the method shall support the test engineer to

assess the flutter proneness e.g. of an aircraft during FVT or an elastic wind tunnel model in a wind tunnel experiment.

3. OUTPUT-ONLY SYSTEM IDENTIFICATION

The basic idea behind several subspace methods is first to estimate the state vector time series $\{x(t)\}$, and then - by linear least squares procedures - to estimate the system matrices. An estimate of the state vector time series may be constructed directly from the response measurements or from the corresponding covariance functions by application of standard linear algebra decompositions such as QR and/or SVD. From these decompositions, it is also possible to obtain the system matrices directly without actually computing the state vector time series. The SSI technique that is presented in section 3.2 is the classical data-driven stochastic realization algorithm.

3.1. State-Space Modelling of Aeroelastic Systems

The FEM is one of the most common tools for modeling mechanical structures and yields stiffness and mass matrices. In case of attached flow the vibrating structure induces aerodynamic loads, which act as additional stiffness, damping or mass. Dependent on its unsteady character, they might lag with respect to the deflection of the structure. For the aeroelastic application, the well-known Doublet-Lattice Method (DLM) can provide the aerodynamic pressure loads in the frequency-domain [11], which can then be transformed to the time-domain using the rational polynomial fit [12]. In the case of a linear dynamic model with linear aerodynamics, one has the following system of ordinary differential equations:

$$\begin{aligned}&[M]\{\ddot{u}(t)\}+[C]\{\dot{u}(t)\}+[K]\{u(t)\}-q_\infty\left[Ae(\{\ddot{u}\},\{\dot{u}\},\{u\},M_\infty)\right]=\{f(t)\}\\&\{y(t)\}=[Ca]\{\ddot{u}(t)\}+[Cv]\{\dot{u}(t)\}+[Cd]\{u(t)\}\end{aligned} \tag{1}$$

where $[M]$, $[C]$ and $[K]$ are the mass, damping and stiffness matrices, respectively, $[Ae]$ is the aerodynamic force matrix, which depends on the vector of nodal displacements $\{u(t)\}$, nodal velocities $\{\dot{u}(t)\}$, nodal acceleration $\{\ddot{u}(t)\}$ and the Mach number M_∞. It is scaled with the dynamic pressure $q_\infty=\frac{1}{2}\rho_\infty V_\infty^2$ including the atmospheric density ρ_∞ and the flight velocity V_∞. The transformation of the impulse of the aerodynamic forces into the Laplace-Domain with Laplace variable $s=\sigma+i\omega$ reads

$$\int_0^\infty\left[Ae(t)\right]e^{-st}dt\approx[Ae_0]+[Ae_1]s+[Ae_2]s^2+\sum_{j=1}^{n_\gamma}\left[Ae_{2+j}\right]\frac{s}{s+\gamma_j}. \tag{2}$$

For the rational approximation several real-valued lag-terms γ must be introduced to represent the time delays between maximum deflection and aerodynamic force amplitudes. The time-dependent external excitation forces $\{f(t)\}$ in Eq. (1) might be a combination of inertia and aerodynamic loads. The output vector $\{y(t)\}$ contains the observable response of the aeroelastic system, which might be accelerations, velocities or even strains. The observation matrices $[Ca]$, $[Cv]$, $[Cd]$ present the relation between the internal states and the limited measured output signals, measured by certain sensor types. By simple mathematical manipulation, the aeroelastic model can be converted into a continuous-time state-space model:

$$\begin{aligned}\{\dot{x}\} &= [A_c]\cdot\{x\}+[B_c]\cdot\{f(t)\}\\ \{y\} &= [C]\cdot\{x\}+[D]\cdot\{f(t)\}\end{aligned} \tag{3}$$

where $\{x\}$ is the state vector of the structure, $[A_c]$ the dynamic and $[B_c]$ the input matrix:

$$\begin{Bmatrix}\{\dot{u}\}\\ \{\ddot{u}\}\\ \{\dot{x}_{a1}\}\\ \{\dot{x}_{a2}\}\end{Bmatrix} = \underbrace{\begin{bmatrix} 0 & [I] & 0 & 0\\ -[\bar{M}]^{-1}[\bar{K}] & -[\bar{M}]^{-1}[\bar{C}] & q_\infty[\bar{M}]^{-1}[Ae_3] & q_\infty[\bar{M}]^{-1}[Ae_4]\\ 0 & [I] & -\left(\frac{V_\infty}{b}\right)\gamma_1[I] & 0\\ 0 & [I] & 0 & -\left(\frac{V_\infty}{b}\right)\gamma_2[I]\end{bmatrix}}_{[A_c]} \begin{Bmatrix}\{u\}\\ \{\dot{u}\}\\ \{x_{a1}\}\\ \{x_{a2}\}\end{Bmatrix} + \underbrace{\begin{bmatrix}0\\ -[\bar{M}]^{-1}\\ 0\\ 0\end{bmatrix}}_{[B_c]}\{f(t)\} \tag{4}$$

$$[\bar{M}]=[M]-q_\infty[Ae_2]\left(\frac{b}{V_\infty}\right)^2,\quad [\bar{C}]=[C]-q_\infty[Ae_1]\left(\frac{b}{V_\infty}\right),\quad [\bar{K}]=[K]-q_\infty[Ae_0]$$

In addition to the structural states $\{x\}^T=\left\{\{u\}^T\ \{\dot{u}\}^T\right\}$, the aerodynamic lag-states $\{x_a\}$ are introduced. The detailed assembly of the aeroelastic system can be found in reference [13] or [14]. The continuous state-space model can be discretized in time with fixed sampling steps

$$\begin{aligned}\{x\}_{k+1} &= [A]\{x\}_k+[B]\{f\}_k+\{w\}_k\\ \{y\}_k &= [C]\{x\}_k+[D]\{f\}_k+\{v\}_k\end{aligned}, \tag{5}$$

where $\{v\}_k$, $\{w\}_k$ are unknown stochastic disturbances. The zero-order hold assumption on the inputs $\{f\}_k$ yields the following relationship between the continuous-time and the discrete-time system:

$$[A]=e^{[A_c](\Delta t)} \quad \text{and} \quad [B]=\left([A]-[I]\right)[A_c]^{-1}[B_c]. \tag{6}$$

If we suppose now, that all system matrices are known, the outputs $\{y\}_k$ can be measured but the inputs $\{f\}_k$ might be unknown and there is some measurement noise, the model of Eq. (5) changes into

$$\begin{aligned}[\{x\}_{k+1} \quad \{x\}_{k+2} \quad \dots \quad \{x\}_{k+p}] &= [A][\{x\}_k \quad \{x\}_{k+1} \quad \dots \quad \{x\}_{k+p-1}]+\{w\}\\ [\{y\}_k \quad \{y\}_{k+1} \quad \dots \quad \{y\}_{k+p-1}] &= [C][\{x\}_k \quad \{x\}_{k+1} \quad \dots \quad \{x\}_{k+p-1}]+\{v\}.\end{aligned} \tag{7}$$

The terms $\{v\}$ and $\{w\}$ are assumed to be of stochastic type with discrete white noise nature and an expected value equal to zero.

3.2. Data-driven Stochastic Subspace Identification Algorithm

In the data-driven SSI, first the recorded output data samples are arranged in the “past” and “future” matrices $[Y^-]$ and $[Y^+]$:

$$\left[Y^{-}\right]=\frac{1}{\sqrt{N}}\begin{bmatrix} y_q & y_{q+1} & y_{q+2} & \cdots & y_{N+q-1} \\ y_{q-1} & y_q & y_{q+1} & \cdots & y_{N+q-2} \\ y_{q-2} & y_{q-1} & y_q & \cdots & y_{N+q-3} \\ \vdots & \vdots & \vdots & \ddots & \vdots \\ y_1 & y_2 & y_3 & \cdots & y_N \end{bmatrix},\quad \left[Y^{+}\right]=\frac{1}{\sqrt{N}}\begin{bmatrix} y_{q+1} & y_{q+2} & y_{q+3} & \cdots & y_{N+q} \\ y_{q+2} & y_{q+3} & y_{q+4} & \cdots & y_{N+q+1} \\ y_{q+3} & y_{q+4} & y_{q+5} & \cdots & y_{N+q+2} \\ \vdots & \vdots & \vdots & \ddots & \vdots \\ y_{q+p+1} & y_{q+p+2} & y_{q+p+3} & \cdots & y_{N+q+p} \end{bmatrix}. \tag{8}$$

The so-called "subspace matrix" or block Hankel matrix $\left[H\right]$ is obtained from the LQ-decomposition of the combined system:

$$\begin{bmatrix}\left[Y^{-}\right] \\ \left[Y^{+}\right]\end{bmatrix}=\begin{bmatrix}\left[R_{11}\right] & 0 \\ \left[R_{21}\right] & \left[R_{22}\right]\end{bmatrix}\begin{bmatrix}\left[Q_1\right] \\ \left[Q_2\right]\end{bmatrix} \quad \text{with} \quad \left[H\right]=\left[R_{21}\right] \tag{9}$$

The covariance between past and future can be found in the lower left part. The observability matrix $\left[O\right]$ is obtained by Singular Value Decomposition (SVD) of $\left[H\right]$, where the singular values can be split in dominating with significant value $\left[S_1\right]$ and insignificant $\left[S_2\right]$. The dominating part determines the rank of the subspace matrix:

$$\left[H\right]=\begin{bmatrix}\left[U_1\right] & \left[U_2\right]\end{bmatrix}\begin{bmatrix}\left[S_1\right] & \\ & \left[S_2\right]\end{bmatrix}\begin{bmatrix}\left[V_1\right]^T \\ \left[V_2\right]^T\end{bmatrix} \rightarrow \left[U_1\right]\left[S_1\right]\left[V_1\right]^T \tag{10}$$

The observability matrix is truncated at the desired model order:

$$\left[O\right]=\left[U_1\right]\left[S_1\right]^{1/2} \quad \text{and} \quad \left[X\right]=\left[S_1\right]^{1/2}\left[V_1\right]^T \tag{11}$$

From the observability matrix $\left[O\right]$ the output matrix $\left[C\right]$ in the first block row and the dynamic matrix $\left[A\right]$ are determined via least-squares solution of

$$\left[A\right]=\left[O_1\right]^{\dagger}\left[O_2\right] \quad \text{with} \quad \left[O_1\right]=\begin{bmatrix}\left[C\right] \\ \left[C\right]\left[A\right] \\ \vdots \\ \left[C\right]\left[A\right]^{p-1}\end{bmatrix},\left[O_2\right]=\begin{bmatrix}\left[C\right]\left[A\right] \\ \left[C\right]\left[A\right]^2 \\ \vdots \\ \left[C\right]\left[A\right]^{p}\end{bmatrix}, \tag{12}$$

where † denotes the Moore–Penrose pseudo-inverse. The data-driven Principal Component (PC) algorithm from [3] is chosen, where the principal angles and directions between the row spaces of the past and futures matrices are determined to build an orthogonal projected subspace matrix in Eq. (9):

$$\left[H\right]=\left(chol\left(\left[R_2\right]\left[R_2\right]^T\right)\right)^{-1}\left[R_{21}\right] \quad \text{with} \quad \left[R_2\right]=\begin{bmatrix}\left[R_{21}\right] & \left[R_{22}\right]\end{bmatrix} \tag{13}$$

This implementation results in clearer separation between physical content of the analyzed signals and their noise.

3.3. Determination of the Modal Parameters

The system's modal parameters comprise eigenfrequencies, damping ratios and mode shapes, which can be calculated from the identified system matrices in Eq. (12). An eigenvalue decomposition of $[A]$ leads to the diagonal matrix $[\Lambda]$ of discrete-time system poles μ_i and corresponding right eigenvectors $\{\psi\}_i$:

$$[A]=[\Psi][\Lambda][\Psi]^{-1} \quad \Rightarrow \quad [A]\{\psi\}_i = \mu_i \{\psi\}_i \tag{14}$$

From Eq. (6), the discrete-time system poles μ_i are related to the continuous-time system poles λ_i by

$$\lambda_i = \frac{\ln(\mu_i)}{\Delta t} \tag{15}$$

The undamped eigenfrequencies f_i and damping ratios ζ_i can be calculated from the continuous-time system poles λ_i:

$$f_i = \frac{|\lambda_i|}{2\pi} \quad \text{and} \quad \zeta_i = -\frac{\mathrm{Re}(\lambda_i)}{|\lambda_i|} \tag{16}$$

The product of the observed part of the eigenvectors $\{\psi\}_i$ and the output matrix leads to the experimental mode shapes $\{\phi\}_i$:

$$\{\phi\}_i = [C]\{\psi\}_i \tag{17}$$

Since the input energy to the system is not measured, the mode shapes cannot be normalized. There are a number of reasons why the SSI algorithm does not yield the exact system matrices $[A]$ and $[C]$, but only estimates :

- Due to the finite number of data samples N, the output covariance matrices cannot be calculated exactly, but only approximated by an estimate.
- The unmeasured inputs and the output measurement noise may not be white noise vectors.
- Due to the limited resolution of the A/D-conversion during the data acquisition, there might round-off errors in the recorded data samples.
- Because all real structures are to some extent nonlinear, nonlinear distortions that are not negligible might be present in the data.
- Since the system order must be chosen in advance, its value might be chosen too low or too high.

3.4. Stabilization Diagram

Traditionally, modal parameters are extracted for a series of increasing model orders up to an over-estimation of the system and the parameters obtained at each order are compared with the ones obtained at the previous order in a stabilization diagram. The model order is related to the number of retained singular values in the approximation of the subspace matrix in Eq. (10). The order

preselection is determined by a minimum threshold $s_{\min}$ of the singular values, which are normalized by the maximum value $s_i \geq s_{\min}$. A selection is then made on the fact that physical modes tend to stabilize from step to step. Stabilization diagrams have proven their efficiency but require an operator to interpret the results for each analysis. In order to perform online-monitoring of aircraft structures for instance, it is obviously not practicable to manually select the poles from the right model order from a stabilization diagram. One way to automatize this procedure is to evaluate the deviation of eigenfrequencies, dampings and mode shapes over model order. The MACXP criteria, proposed by Vacher in [15], expands the well-known Modal Assurance Criteria MAC by a pole-weighting, which takes the deviation of real and imaginary parts of the poles as additional weighting on the correlation of two compared mode shapes.

$$MACXP\left(\phi_i,\phi_j\right)=\frac{\left(\frac{\left|\phi_i^*\phi_j\right|}{\left|\bar{\lambda}_i+\lambda_j\right|}+\frac{\left|\phi_i^T\phi_j\right|}{\left|\lambda_i+\lambda_j\right|}\right)^2}{\left(\frac{\phi_i^*\phi_i}{2\left|\mathrm{Re}\,\lambda_i\right|}+\frac{\left|\phi_i^T\phi_i\right|}{2\left|\lambda_i\right|}\right)\left(\frac{\phi_j^*\phi_j}{2\left|\mathrm{Re}\,\lambda_j\right|}+\frac{\left|\phi_j^T\phi_j\right|}{2\left|\lambda_j\right|}\right)} \tag{18}$$

The MACXP can be interpreted in terms of the correlation function between the real decay responses associated to two modes. Figure 1 shows the comparison between the classical MAC, which only uses the mode shapes, and the MACXP, which provides a more clear correlation.

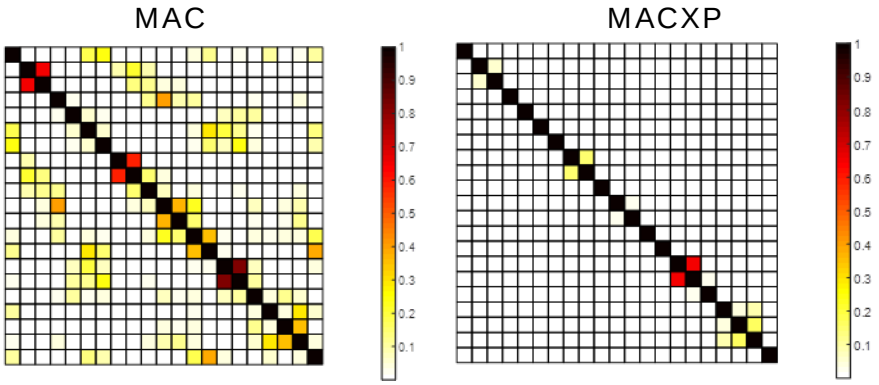

Figure 1. MAC and MACXP plots obtained from correlation of a set of complex modes.

In practice, the SSI procedure of section 3.2 is applied for decreasing truncation order of the SVD in Eq. (10) starting from the user pre-selected maximum system order towards lower orders. The MACXP is evaluated for all identified poles and modes of two successive orders. If a correlation factor occurs higher than a given threshold, then both modes are tracked from the higher model order to the lower one. This procedure is repeated for several model orders to get a robust correlation of the physical poles and modes. Here, the Fast Multi-Order SSI Algorithm 2 procedure from reference [7] is exploited, where the LQ-decomposition of Eq. (13) and the SVD of Eq. (10) is performed only once for the highest model order. Then the least square problem of Eq. (12) can be solved for each model order. Note, that it is not required to continue the analysis down to the lowest model order, since the stabilization of poles can be observed from a limited number of model orders evaluated. This might save computational costs, because then the eigenvalue problem of Eq. (14) must not be solved for each order. For the automatic application such a reduced implementation close to real-time, is mandatory for the analysis to be completed in a given time window, e.g. the time interval in which new response date is made available for analysis.

Now the question arises, from which model order the system matrices $[A]$ and $[C]$ should be chosen by the automatic algorithm. To build a consistent representation, it is advisable to use the lowest possible model order, which still contains all physical poles, which were identified at the maximum order. Physical poles are identified as stable poles at least in the first five model orders. By following this constraint, the overestimation of the system analysis in Eq. (10) is reduced to a minimum. On the

other hand, it can be granted that all identified modal parameters are solutions from only one matrix pair. The search algorithm can be easily implemented in the procedure to generate the stabilization diagram.

3.5. Time Data Reduction

In general, the acquisition of the time histories is carried out with a fixed sample rate f_s, which should be a multiple of the highest frequency under investigation. Since the number of samples in the analyzed time window determine the size of the block Hankel matrix in Eq. (9), the LQ-decomposition should be performed for a minimized system to save computation time. Hence, a resampling procedure should assure that the sampling rate is reduced to twice of the estimated maximum eigenfrequency $f_{\max}$ of the mode shape to be identified. This requires digital low pass filtering of the raw time histories before down-sampling with every n-th sample:

$$n = fix\left(\frac{f_s}{2f_{\max}}\right). \tag{19}$$

Here, a Butterworth filter is applied to all measured response signals. In case of the measurement of accelerations the higher frequencies are dominating the total response. It is required to analyze the system at high model orders in Eq. (10) to identify physical poles also at low frequencies. By previous down-sampling, computational effort can be reduced to a minimum, which is important for the fast application in online monitoring.

4. CASE STUDIES

The presented SSI-based identification process is coded within *MATLAB*. With the following two case studies its robust and fast execution will be demonstrated for the utilization in the GVT and the FVT.

4.1. Ground Vibration Test of Glider Aircraft

To identify the modal parameters of a doubled-seated glider aircraft shown in Figure 2 the prototype was instrumented with 83 accelerometers as plotted in Figure 4 to measure the in-plane and out-of-plane motions of all lifting surfaces. The span-wise deformations are used to calculate the motion-induced aerodynamic forces, which might then be exploited in the flutter analysis. The glider is softly suspended by rubber bungees to simulate the free flight condition (see Figure 3). During the first part of the ground vibration test all structural mode shapes were excited mono-frequently by shakers to isolate eigenfrequencies, mode shapes, damping ratios and modal mass with best accuracy.

The frequency is manually tuned by the test engineer to maximize the Mode Indicator Function MIF for each identified mode:

$$MIF = 1000\left(1 - \frac{\sum_m \left|\mathrm{Im}\left(\phi_m\right)\right|\left|\phi_m\right|}{\sum_m \left|\phi_m\right|^2}\right) \tag{20}$$

The investigation by the Normal Modes Tuning took about one working day.

Subsequently, the aircraft was excited in sine-on-random testing for 500 seconds by three shakers as shown in Figure 5 to apply non-coherent force spectra in the 1-60Hz range. The structural response was recorded with a sample rate of 200Hz and then analyzed with SSI, where the input parameter selection is summarized in Table 1. Figure 7 shows the resulting stabilization diagram with all identified poles above and with cleaned poles below, where the MACXP criteria of 0.95 was applied. The maximum model order of 345 results from the maximum threshold of 0.9 of the normalized singular value.

Figure 2. Glider aircraft during maiden flight.

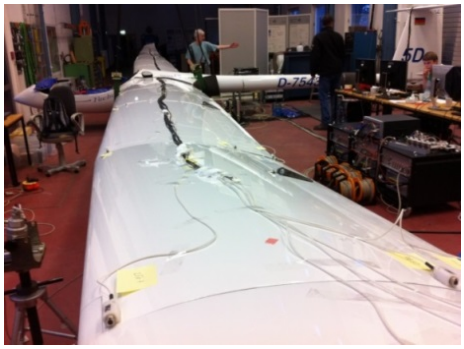

Figure 3. Glider aircraft during GVT.

Table 2 comprises the frequencies, damping ratios and modal indicator functions MIF of the first 21 identified physical poles in the range between 2.69 and 37.56Hz. As examples, three mode shapes of the aircraft are plotted in Figure 6: fundamental symmetric, 1st antisymmetric and 2nd wing bending. All MIF-values show good quality up to 23.6Hz. Above, the impact of the mechanical control system becomes stronger, where especially the wing control surfaces do not vibrate in phase with the overall wing. Mode 17 is a pure aileron mode, while mode 18 and 19 are the symmetric and antisymmetric wing torsion, respectively, where the ailerons contribute. The MAC-plot and the MACXP-plot of all 21 modes were already presented in Figure 1. The orthogonality is more accentuated by the MACXP, where two or less similar modes are separated by the complex poles.

In addition, Table 2 contains the corresponding frequencies of the Normal Modes Tuning and the MAC-values between sine-dwell and sine-on-random testing are given. Again, the correlation shows very good agreement up to mode 16. Above the free-play effects of the control system are observable, which contaminate the modal results.

The SSI-analysis takes not more than 30 seconds on a portable computer with customary *Intel Core i7* processor. In total, the fully automatic experimental modal analysis takes about 15 minutes at maximum including acquisition time. This needs to be compared to one working day with the Normal Modes Tuning method, which clearly demonstrates the potential of the presented process.

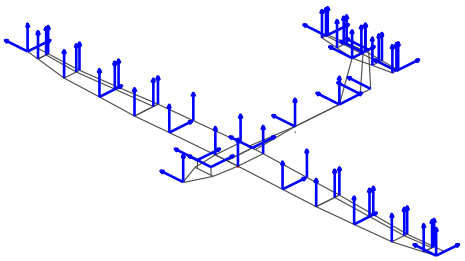

Figure 4. Sensor plan.

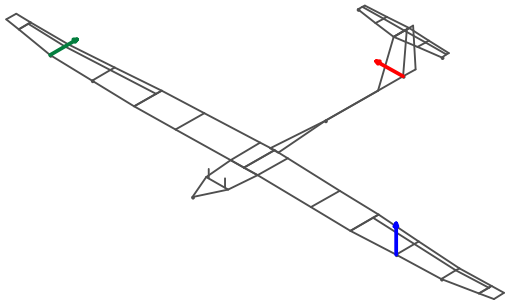

Figure 5. Shaker for random excitation.

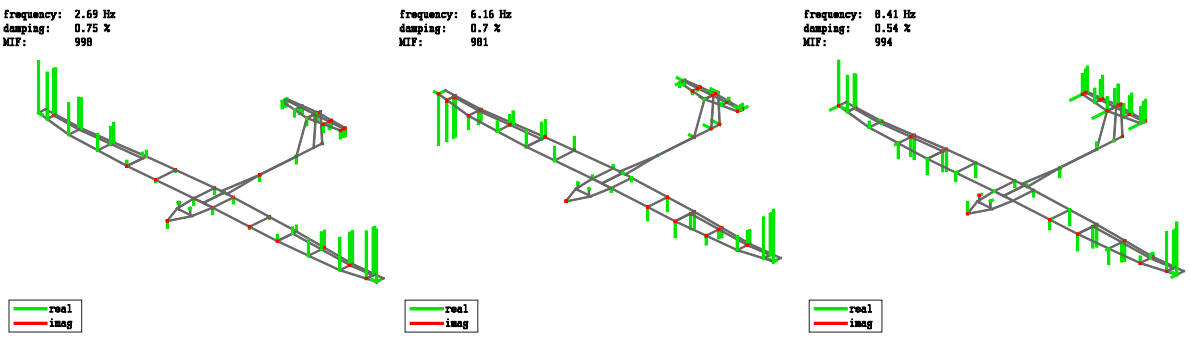

Figure 6. Identified mode shapes of glider aircraft.

Table 1. SSI-input parameter selection.

No. of channels	83
Sampling frequency	200 Hz
No. of samples	1e6
cut-off frequency	40 Hz
order of Butterworth filter	5
No. of time blocks *p*	8
threshold of normalized singular value	0.9
lower threshold of MACXP	0.95
time for LQ-decomposition	5.57s
time for SVD-decomposition	0.17s
time for stab. diagram (system order = 354)	25.54s
total time	31.27s
best model order	345

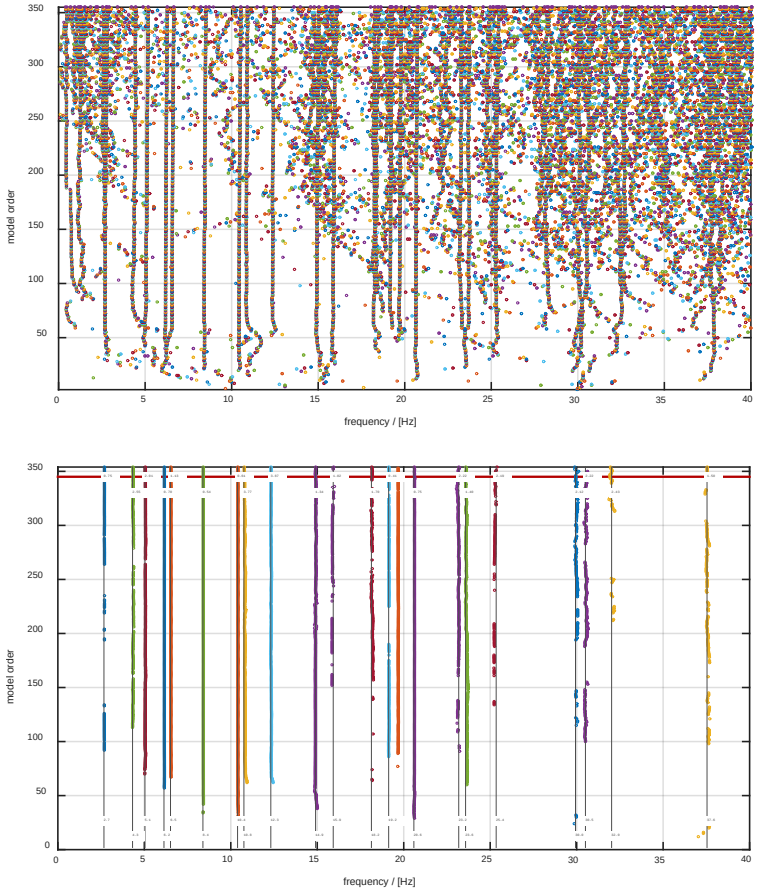

Figure 7. Un-cleaned and MACXP-cleaned SSI-stabilization diagram.

Table 2. SSI-identified modal parameters and comparison with Normal Modes Tuning.

	SSI				Normal Modes Tuning		SSI				Normal Modes Tuning
Mode	frequency [Hz]	damping [%]	MIF	MAC	frequency [Hz]	Mode	frequency [Hz]	damping [%]	MIF	MAC	frequency [Hz]
1	2.69	0.75	998	100	2.66	12	18.15	1.70	919	95	18.16
2	4.34	2.55	971	97	4.49	13	19.15	0.41	864		
3	5.06	2.01	942	95	5.45	14	20.61	0.75	978	99	20.58
4	6.16	0.70	981	100	6.15	15	23.20	2.22	843		
5	6.54	1.13	976	99	6.47	16	23.60	1.40	968	97	23.39
6	8.41	0.54	994	100	8.39	17	25.36	2.19	171	47	24.15
7	10.42	0.61	967	99	10.37	18	29.95	2.12	686	87	29.84
8	10.78	3.77	935	98	10.79	19	30.52	2.22	670	83	29.61
9	12.33	3.87	889	97	12.49	20	32.04	2.43	417	53	32.35
10	14.93	1.34	914	96	14.93	21	37.56	1.50	882	93	38.11
11	15.95	1.02	930	97	15.84						

4.2. Flight Vibration Test of Research Aircraft

HALO is the high altitude and long range research aircraft for the German atmospheric research community. The research aircraft is based on a commercial business jet and has been customized to cover the requirements for its special mission profile. Modifications comprise a nose boom, view ports, apertures as well as external stores which can be mounted at fuselage and wing hard points. The concept behind HALO is to provide an optimal platform for airborne atmospheric science and Earth observation, a well-equipped flying laboratory.

For the first scientific mission, the HALO aircraft was equipped with a large belly pod for atmospheric experiments, which requires a ventral fin to restore sufficient yaw stability (see Figure 8).

Although no rapid loss of damping was expected, the ventral fin might have impact on the unsteady aerodynamics induced by vibration modes of the overall empennage. For the flight tests the HALO research aircraft was instrumented with accelerometers at both wing tips, vertical tail tip, fuselage nose and mid wing, as depicted in Figure 9. No external exciter system and no telemetry was available, so the aeroelastic test engineer was on-board during the test flights to perform the damping monitoring and the aircraft could be well excited by pilot rudder kicks and aileron jerks. All acceleration signals were continously logged together with the current flight conditions including flight speed, Mach number and flight altitude with sample rate of 200 Hz. Figure 10 shows the typical profile of a flight test, where the pilot tries to hold a fixed altitude during pre-defined sections, while the flight speed is varied. In general, the Mach number is increased and reduced, starting at a safe flight speed. Then the pilot climbs up to the next test altitude.

Since the implementation of the presented SSI-method was not available at this particular time, the automatic online evaluation of the flight test was subsequently simulated based on the logged test data. The recorded raw acceleration time series are analyzed in time windows of 60 seconds, shifted by 5 seconds in each step, where the parameters for SSI are chosen as following:

- number of time blocks: 15,
- upper threshold of normalized singular value: 0.9,
- lower threshold of MACXP: 0.7.

So, in the real flight test situation the flight test engineer will have a new OMA result every 5 seconds on his screen. The MACXP criteria from Eq. (18) is not only used to clean the stabilization diagram and to find the physical poles, it is also applied to track the modes between a pre-sequent modal result and a new evaluation at slightly varying Mach Number and flight altitude. In Figure 11 all identified damping values and frequencies are plotted over the Mach number for the highest altitude plateau in 12500 m, as part of the test flight plotted in Figure 10. There are 570 evaluations of the SSI-method during this flight section. From the mode correlation a restricted cubic spline of the mean values can be obtained via least squares method from [16] to fit the mean values along the flight speed. In addition, the 95% confidence intervals of the mean values (shaded areas) are calculated based on the bootstrap procedure.

Figure 8. HALO aircraft with belly pod.

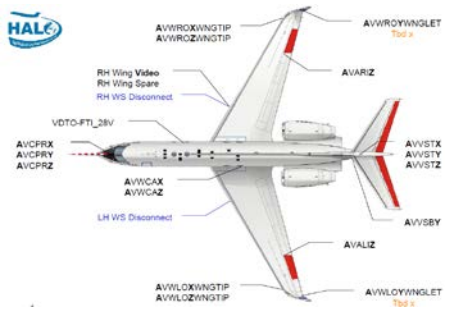

Figure 9. FTI Flight Test Instrumentation.

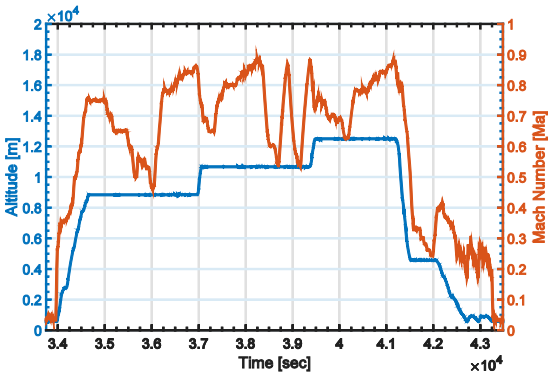

Figure 10. Altitude and Speed in typical test flight.

In case of the identified frequencies the confidence bands are rather slight, if there are a lot of test points. The bands are fast expanding, if only a few samples are available, which is especially the case for the antisymmetric modes, because they are not so well excited during straight flight in the atmosphere without turbulence. This is why the pilot has to excite the aircraft with rudder kicks and aileron jerks. In case of identified damping, the scatter is significantly higher. Some outliers are located near the zero damping line, which is the limit for the flutter stability. On the other hand, the confidence bands of the mean values can show clear damping trends for increasing flight speed. Especially, the mean damping loss of the most flutter critical mode with lowest frequency is observable in the range M = 0.75-0.88. The restricted cubic spline is applied for extrapolation towards higher Mach number. While the mean values show clear trends, the 95% confidence bands of the mean values expand, since the uncertainty increases with larger distance to the measured test points.

The fully automatic identification procedure via SSI and MACXP needs about 3 seconds for the analysis of each 60 seconds time window with 17 signals running on a commercial Notebook with *Intel Core i7* processor. As a conclusion, it can be stated, that the presented online monitoring procedure might be a valuable tool for the FVT to support the test engineers by rapidly assessing the flutter proneness of the aircraft in the current flight condition.

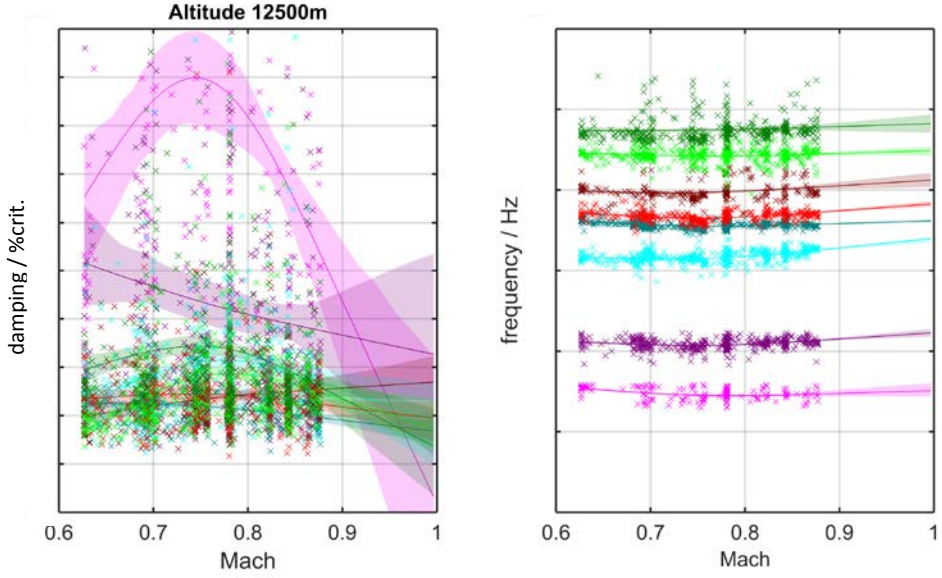

Figure 11. SSI-identified frequencies and dampings from flight test data.

5. SUMMARY AND CONCLUSIONS

The fully automatic process for operational modal analysis OMA using output-only data was presented with theory and application to aeroelastic identification problems. The process is based on the Stochastic Subspace Identification SSI expanded by methods to automatically generate the stabilization diagram and select the physical poles by exploiting the MACXP criteria over a range of model orders. The fast and robust utilization is presented by means of a ground vibration test GVT example and the simulation of a flight vibration test FVT based on real test data recorded in flight. Here it can be demonstrated, that in case of the GVT the testing time can be reduced significantly without loss of result quality of the identified modal parameters. In case of the FVT it can be demonstrated, that a continuous monitoring of frequencies and dampings of the aircraft during the test flight is possible.

The method has the potential to support the flight test engineers and the test pilot in safely and efficiently conducting FVT. In fact, due to availability of OMA results of aeroelastic systems in real-time, tracking of the eigenfrequencies and damping ratios is enabled e.g. as function of flight speed, flight altitude, fuel burn, or even other environmental parameters. When applying this method, there is generally no requirement for specific excitations in flight to be conducted at discrete points in the

flight envelope, since no reference to system inputs is evaluated. Therefore, this method can contribute to significantly reduce the duration of flight tests and consequently also reducing the cost. Most importantly, the test pilot is supported by some objective estimates of the current damping of the aircraft. Currently, the extrapolation of eigenfrequencies and damping ratios is pursued. It is desired to quantify the flutter safety margin during the on-going FVT with update rates of eigenfrequencies, damping ratios and flutter safety margin close to real-time.

6. ACKNOWLEDGEMENT

The authors like to thank the *Akademische Fliegergruppe Darmstadt* for providing the glider aircraft *D43* and for supporting the ground vibration test. Further, the support of the flight test team of DLR *Flight Experiments* in Oberpfaffenhofen is gratefully acknowledged. Thanks to the DLR scientific research project *ALLEGRA* the code implementation of the SSI-based OMA-method could be developed.

7. REFERENCES

[1] Meijer, J.J. (2005). *Introduction to Flight Test Engineering - "Aeroelasticity"*. RTO AGARDograph 300 Vol. 14 (2005).

[2] Schwochow, J. und Zöger, M. (2013). *Flight vibration testing - we always did it this way*. 24rth SFTE-EC Symposium, 11.-13. Juni 2013, Braunschweig, Germany.

[3] Van Overschee, P., De Moor, B. (1996). *Subspace identification for linear systems: Theory, implementation, applications*. Kluwer Academic Publishers, 1996.

[4] Tasker, F., Bosse, A., Fisher, S. (1998). *Real-Time Modal Parameter Estimation using Subspace Methods: Theory*. Mechanical Systems and Signal Processing (1998) 12(6), 797-808.

[5] Bosse, A., Tasker, F., Fisher, S. (1998). *Real-Time Modal Parameter Estimation using Subspace Methods: Applications*. Mechanical Systems and Signal Processing (1998) 12(6), 809-823.

[6] Brincker, R., Andersen, P. (2006). *Understanding Stochastic Subspace Identification*. Proceedings of the 24th International Modal Analysis Conference (IMAC), St. Louis, Missouri, 2006.

[7] Doehler, M., Mevel, L. (2010). *Fast Multi-Order Stochastic Subspace Identification*. INRIA Research Report RR-7429, 2010. <inria-00527484>.

[8] Goursat, M., Doehler, M., Mevel, L., Andersen, P. (2010). *Crystal Clear SSI for Operational Modal Analysis of Aerospace Vehicles*, 28th International Modal Analysis Conference IMAC-XXVIII, 2010.

[9] Van der Auweraer, H.; Peeters, B. (2004). *Discriminating physical poles from mathematical poles in high order systems: use and automation of the stabilization diagram*, Instrumentation and Measurement Technology Conference, 2004. IMTC 04. Proceedings of the 21st IEEE , vol.3, no., pp. 2193- 2198 Vol.3, 18-20 May 2004.

[10] Jelicic, G., Schwochow, J., Govers, Y., Böswald, M., Hebler, A (2014). *Real-time assessment of flutter stability based on automated output-only modal analysis*. ISMA, Leuven, Belgium.

[11] Rodden, W.P., Albano, E. (1969). *A Doublet-Lattice Method for Calculating Lift Distributions on oscillating Surfaces in subsonic Flows*. AIAA Journal. Vol. 7, No. 2, pp. 279-285 (1969).

[12] Roger, K. L. (1977). *Airplane Math Modeling Methods for Active Control Design. Structural Aspects of Active Controls*, AGARD-CP-228, Aug. 1977.

[13] Gupta, K.K. (1997). *Development and Application of an Integrated Multidisciplinary Analysis Capability*. International Journal for Numerical Methods in Engineering, Vol. 40, pp. 533-550 (1997).

[14] Karpel, M. (2001). *Procedures and Models for Aeroservoelastic Analysis and Design*. ZAMM Z. Angew. Math. Mech. 81 (2001) 9, pp. 579-592.

[15] Vacher, P., Jacquier, A., Bucharles, A. (2010). *Extensions of the MAC criterion to complex modes*. In Proceedings of ISMA 2010.

[16] Harrell, F. E. Jr. (2001). *Regression Modelling Strategies (With application to linear models, logistic regression and survival analysis).* 2001, Springer Series in Statistics, pages 20-21.